Na, Mg and Al abundances as a population discriminant for nearby metal-poor stars [*]

T. Gehren[1], J.R. Shi[1,2], H.W. Zhang[1,3], G. Zhao[1,2], and A.J. Korn[1,4]

[1] Institut für Astronomie und Astrophysik der Universität München, Scheinerstr. 1, D-81679 München, Germany
[2] National Astronomical Observatories, Chinese Academy of Sciences, Beijing 100012, P.R. China
[3] Department of Astronomy, School of Physics, Peking University, Beijing 100871, P.R. China
[4] Uppsala Astomical Observatory, Box 515, 75120 Uppsala, Sweden

ABSTRACT

Aims. Parameters for 55 nearby metal-poor stars are determined using high-resolution spectroscopy. Together with similar data taken from a recent analysis, they are used to show trends of their Galactic evolution with stellar [Fe/H] or [Mg/H] abundances. The separation of abundance ratios between disk and halo stars is used as a basic criterion for population membership.
Methods. After careful selection of a clean subsample free of suspected or known binaries and peculiar stars, abundances of Mg, Na and Al are based on NLTE kinetic equilibrium calculations applied to spectrum synthesis methods.
Results. The relation between [Na/Mg] and [Fe/H] is a continuous enrichment through all three Galactic populations spanning a range of values between a metal-poor plateau at [Na/Mg] = –0.7 and solar values. [Al/Mg] displays a step-like difference between stars of the Galactic halo with $\overline{[Al/Mg]} \sim -0.45$ and the two disk populations with $\overline{[Al/Mg]} \sim +0.10$. [Al/Mg] ratios, together with the [Mg/Fe] ratios, asymmetric drift velocities V, and stellar evolutionary ages, make possible the individual discrimination between stars of the thick disk and the halo. At present, this evidence is limited by the small number of stars, and by the theoretical and empirical uncertainties of stellar age determinations, but it achieves a high significance.
Conclusions. While the stellar sample is not complete with respect to space volume, the resulting abundances indicate the necessity to revise current models of chemical evolution to allow for an adequate production of Al in early stellar generations.

Key words. Line: formation - Line: profiles - Stars: abundances - Stars: late-type - Galaxy: evolution

1. Introduction

Stellar populations were originally recognized and defined according to their kinematic properties (Oort 1926; Baade 1944; Roman 1955), and it was not until Eggen, Lynden-Bell and Sandage (1962) that kinematic data were correlated with mean metal abundances. In a first attempt to understand the formation of the Galaxy, their investigation established the meaning of eccentric stellar orbits as well as that of the asymmetric drift velocity. At about the same time, Wallerstein (1961) recognized that there is some evidence for non-solar abundance ratios of the α-elements, particularly in kinematically extreme stars of population II, which then was related to the stellar component of the Galactic halo. Later, Gilmore and Reid (1983) found that the Galactic disk, originally associated with population I stars, is actually composed of two (sub)populations, a *thin* and a *thick disk*.

At that time, the topic was controversial (see e.g. Bahcall & Soneira 1984, Bahcall et al. 1985), and even today the notion of a third Galactic population is not very popular among some astronomers. Roughly ten years later, Edvardsson et al. (1993) presented a first comprehensive abundance analysis of disk stars resulting in a more or less smooth change of individual element abundance ratios [X/Fe][1]. While this chemical enrichment was interpreted as a continuous evolution of stellar generations, the first clear separation of thin and thick-disk stars was presented by Fuhrmann (1998, 2004) who was able to show that the thick disk is a distinct stellar component, both in terms of abundances and age, whereas the kinematic properties are by far less conclusive when looking for an old metal-poor population. Moreover, he gives evidence for the speculation that the thick disk is not at all a *minor* component of the Milky Way, and that instead the halo component, i.e. the original population II, consists of only a very few objects if it is a separate population at all. Fuhrmann shows that the distinction

---

[1] As usual, $[X/Fe] = \log(N_X/N_{Fe}) - \log(N_X/N_{Fe})_\odot$ represents the normalized logarithmic abundance ratio of elements X and Fe
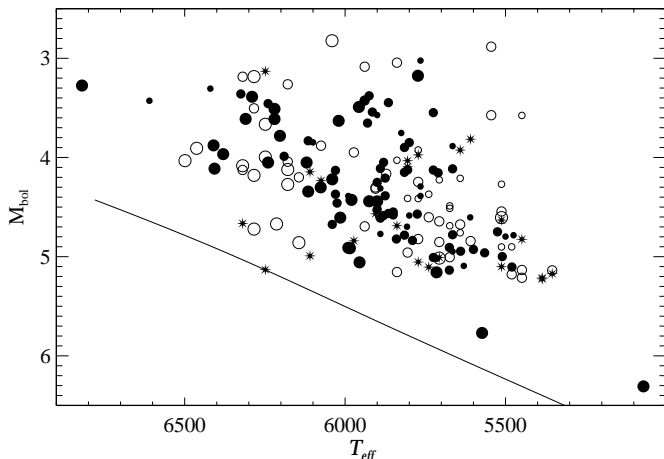
Fig. 1. Temperature-magnitude diagram of unevolved near-turnoff stars, based on HIPPARCOS parallaxes. Filled circles refer to stars observed, open circles to the rest of the sample with temperatures approximated from a simple B–V vs. T_{eff} correlation. Symbol sizes increase with the δ(U–B) excesses in the three intervals [0.10 - 0.14], [0.14 - 0.20] and >0.20 . Star symbols denote peculiar stars (binaries etc.). The zero age main sequence for [Fe/H] = −1.5 is plotted for comparison. The two stars at the extreme left are G9-16 and HD 128167, that on the lower right is HD 103095

between stars of thin and thick disk requires a careful determination of the [Mg/Fe] ratio.

Other element ratios have been investigated in thick-disk stars by Gratton et al. (2000) and Prochaska et al. (2000) who confirm the separate nature of the thick disk. Generally, the roughly constant [Mg/Fe] ∼ 0.4 overabundance found among thick-disk stars has convinced many authors to accept that this stellar component must have formed on a short (SN II) time scale of < 1 Gyr. The age determinations supplied by Fuhrmann also seem to indicate that the thick disk is nearly as old as the Galaxy itself, and that star formation stopped for a few billion years before the formation of the thin disk started. In combination with his unexpected high mass density estimate of the thick disk, it would not leave a central role for the Galactic halo. A closer examination of Fuhrmann's data, however, reveals a weak trend in the chemical evolution of the thick disk [Fe/Mg] ratio (see Fig. 34 in Fuhrmann 2004). Such a trend is more clearly visible in the [Ba/Eu] ratios presented by Mashonkina et al. (2004) which indicates the onset of s-process contributions from stars of significantly lower masses. Thus, both the Fe/Mg and the Ba/Eu enrichment in thick-disk stars must be interpreted in terms of nuclosynthesis different from that in SN II alone.

As is the case with the distinction between thin and thick disk, there exists a floating boundary between thick disk and halo, as far as kinematics and metal abundances are concerned. Concepts of *metal-weak thick-disk stars* or *metal-rich halo stars* have occasionally been debated with no real definition of their properties. Still, the most reliable discrimination is possible for the more extreme cases of very metal-poor stars such as those found recently in large surveys or stars with retrograde Galactic orbits. However, such stars are extremely rare, and the bulk of stars with halo kinematics has metal abundances be-

tween [Fe/H] = −2.5 and −0.6 (see Laird et al. 1988), at least in the local space volume. Recent spectroscopic abundance results have started to establish more reliable measures to identify the very first stages of Galactic evolution. Mashonkina et al. (2004) found a significant offset of the [Eu/Mg] ratios of stars commonly attributed to the Galactic halo with respect to the thick disk, and Gehren et al. (2004, Paper I) present a similar gap for the [Al/Mg] ratio. Both results refer to the abundances of elements or isotopes that depend on enhanced neutron fluxes, but the logarithmic abundance ratios of [Eu/Mg] and [Al/Mg] are of *opposite* sign. As yet no explanation has been found for these trends.

The above abundance results are obtained with refined atomic models and corresponding NLTE calculations. It has been emphasized that in particular Na and Al are extremely sensitive to deviations from LTE. Consequently, all previous LTE abundance analyses of these elements are obsolete for stars less metal-rich than the Sun as was shown in Paper I. Here, we report new NLTE abundance analyses of metal-poor stars selected for their high proper-motion and UV excess (see Paper I, for a full description of the sample). Fig. 1 displays the stars observed and analyzed as well as those left for future analyses. In this paper, Sect. 2 describes the newly observed spectra, Sect. 3 gives short comments on the atmospheric models, the stellar parameters derived from spectroscopy, the atomic models and the NLTE calculations. Sect. 4 presents the abundance results for the new stars, in Sect. 5 we discuss the implications for stellar populations and nucleosynthesis, followed by a short section of conclusions.

2. Observations

High-resolution spectra for 63 stars have been obtained with the FOCES échelle spectrograph at the Calar Alto 2.2m telescope during observing runs in February and June 1999, May 2000, March 2002 and January 2003. Most of the exposures were taken with the 24μ CCD resulting in a nominal 2-pixel spectral resolution of ∼ 40000. In some exposures the resolution was slightly lower due to an increased slit-width allowing for bad seeing and transparency. For a better comparison with more metal-poor stars some subdwarfs were observed with the 15μ CCD resulting in R ∼ 65000. Most of the exposures cover a spectral range from 3900 to 9000 Å, and for most stars the observations were split into at least three single exposures with a maximum of 1800 s integration each. The basic observational data are given in Table 1, where the last four stars are not members of the standard sample. Parallaxes (mas) and proper motions (mas/y) are taken from the HIPPARCOS catalogue (Perryman et al. 1997). N and t_{exp} refer to the number of spectra taken and the total exposure time (s). Data reduction has been described in Paper I. Here, we mention only that the increased redundancy resulting from multiple exposures guarantees optimal spectroscopy. In particular the outstanding continuum definition resulting from the FOCES fibre coupling is important for the determination of Balmer line profiles. The S/N ratio near Hα is in most cases around 200, with exceptions for some of the fainter objects, for which it may be as low as 100.

Table 1. Spectra obtained with the FOCES echelle spectrograph at the Calar Alto 2.2m telescope. See text for further explanations

| Star	Hip	α(2000)	δ(2000)	V	B–V	π	$\sigma(\pi)$	$\mu(\alpha)$	$\mu(\delta)$	N	t_{exp}	
G78-1	12579	02 41 45.70	+47 21 03.8	9.16	0.520	14.51	1.28	50.65	−288.40	1	3600	SB1
HD 17948	13665	02 55 56.74	+61 31 15.8	5.59	0.445	37.78	0.69	145.07	30.84	5	960	-
HD 19445	14594	03 08 25.72	+26 19 58.7	8.04	0.486	25.85	1.14	−209.55	−830.33	2	3600	-
HD 22309	16788	03 36 03.35	+16 28 05.1	7.65	0.580	22.25	1.14	−284.52	−276.33	3	2100	-
HD 22879	17147	03 40 21.66	−03 12 59.3	6.68	0.554	41.07	0.86	689.67	−214.34	3	780	-
HD 30649	22596	04 51 43.24	+45 50 07.9	6.94	0.586	33.44	1.12	376.09	−564.90	2	3400	-
G84-29	23344	05 01 16.53	+04 06 38.3	9.79	0.413	7.80	2.09	154.34	−146.31	1	3600	-
HD 241253	24030	05 09 56.80	+05 33 27.4	9.71	0.520	10.29	1.66	271.40	−70.78	5	8630	-
G96-35	25137	05 22 45.98	+47 54 50.6	9.23	0.590	16.14	1.29	−178.45	−153.78	6	10800	SB2
HD 243357	25361	05 25 27.87	+32 24 42.9	9.73	0.614	11.76	1.89	157.24	−181.56	4	7200	-
HD 36283	25860	05 31 13.80	+15 46 27.7	8.64	0.669	18.66	1.35	−43.48	−373.23	3	3600	-
G99-21	26617	05 39 27.29	+03 57 04.8	10.35	0.640	8.32	2.41	255.83	−243.74	2	3600	-
HD 250792	28671	06 03 14.45	+19 21 44.1	9.28	0.646	14.86	2.50	666.60	−623.13	2	3600	-
HD 46341	31188	06 32 37.84	−06 29 18.6	8.60	0.562	16.86	0.98	256.36	7.32	3	3900	-
HD 56513	35377	07 18 28.77	+27 15 11.6	8.02	0.627	28.19	1.34	156.11	−157.81	4	3600	-
HD 58551	36152	07 26 50.45	+21 32 08.6	6.54	0.464	32.43	0.91	−312.96	−27.00	7	4400	-
HD 59374	36491	07 30 29.00	+18 57 44.4	8.48	0.538	20.00	1.66	29.21	−436.67	7	9600	-
HD 59984	36640	07 32 05.82	−08 52 51.3	5.90	0.540	33.40	0.93	−92.20	−167.52	5	1360	-
HD 60319	36849	07 34 35.10	+16 54 06.6	8.94	0.500	12.15	1.24	5.17	−295.42	3	5400	-
G87-47	36936	07 35 33.86	+35 57 11.0	10.31	0.660	9.97	5.50	261.58	27.58	5	9000	SB2
G40-8	39893	08 08 54.45	+24 37 29.6	9.64	0.681	12.08	2.58	0.35	−384.92	6	10800	SB1
HD 69611	40613	08 17 29.43	−03 59 18.8	7.74	0.584	20.46	1.16	−145.07	−438.72	2	6300	-
HD 233511	40778	08 19 22.61	+54 05 15.1	9.73	0.484	10.36	1.47	−34.50	−628.92	4	7200	-
G9-16	42887	08 44 24.76	+24 47 50.8	9.32	0.316	6.59	1.45	−112.94	−347.99	1	2400	-
HD 84937	48152	09 48 55.87	+13 44 46.1	8.33	0.399	12.44	1.06	373.81	−774.75	2	6900	-
G235-45	48209	09 49 43.41	+65 18 17.3	9.70	0.667	11.57	2.36	−423.93	−260.04	5	7680	-
HD 88446	49988	10 12 19.17	+17 17 59.1	7.88	0.552	14.43	1.11	−155.61	−229.93	5	4200	-
HD 88725	50139	10 14 08.20	+03 09 08.2	7.75	0.609	27.67	1.01	230.37	−400.32	3	2100	-
HD 91784	51897	10 36 10.79	+15 52 20.9	9.09	0.600	14.59	1.33	99.47	−218.85	4	7200	-
G119-32	52771	10 47 23.04	+28 24 03.1	10.26	0.506	10.55	1.75	178.80	−825.79	2	3600	-
G58-23	52958	10 49 52.80	+20 29 30.6	9.94	0.600	11.16	1.70	−239.83	−65.28	9	16200	SB1
HD 94028	53070	10 51 28.29	+20 16 43.0	8.21	0.498	19.23	1.13	−261.86	−456.33	2	4800	-
HD 96094	54196	11 05 15.73	+25 12 07.4	7.60	0.594	16.68	1.00	−400.50	−62.33	4	4800	-
HD 97855A	55044	11 16 03.88	+52 46 22.9	6.51	0.437	25.55	1.39	159.82	56.75	7	4200	VB
BD+20 2594	55592	11 23 16.43	+19 53 40.4	9.97	0.494	8.72	1.57	−326.99	−316.17	3	5400	-
HD 101177	56809	11 38 45.39	+45 06 30.2	6.29	0.566	42.94	0.95	−593.87	14.80	2	1800	-
HD 104056	58443	11 59 03.02	−04 46 37.4	9.01	0.581	12.71	1.23	111.19	−176.84	3	5400	-
HD 104800	58843	12 04 05.53	+03 20 31.7	9.21	0.585	15.97	1.26	58.76	−575.48	3	5400	-
HD 107582	60268	12 21 28.50	+61 44 52.4	8.23	0.622	24.27	0.79	−300.60	−262.21	3	3300	SB?
HD 108076	60551	12 24 46.33	+38 19 06.9	8.03	0.585	26.94	0.82	−587.37	64.53	3	3600	-
HD 108754	60956	12 29 42.93	−03 19 53.8	8.99	0.703	19.20	1.13	−328.02	−562.64	3	5400	SB1
HD 110897	62207	12 44 59.68	+39 16 42.9	5.95	0.557	57.57	0.64	−359.75	139.32	2	1200	-
HD 114606	64345	13 11 21.71	+09 37 31.2	8.72	0.622	16.36	1.15	−520.57	267.23	3	5400	-
HD 114762	64426	13 12 20.10	+17 31 01.7	7.30	0.525	24.65	1.44	−582.69	−1.98	2	4200	-
HD 118659	66509	13 38 00.39	+19 08 55.9	8.81	0.668	18.98	1.22	133.50	−321.73	4	5800	-
G63-46	66665	13 39 59.51	+12 35 24.2	9.37	0.598	7.44	1.70	111.20	−285.84	1	3600	-
HD 119288	66860	13 42 12.98	+08 23 19.0	6.16	0.418	27.96	0.75	−377.86	−87.16	4	2100	-
G165-39	68321	13 59 09.42	+33 51 43.1	10.05	0.410	5.37	1.60	89.09	−429.19	1	1800	-
HD 123710	68796	14 04 57.39	+74 34 24.1	8.21	0.590	22.84	0.68	−147.22	90.12	4	4800	-
HD 126512	70520	14 25 30.04	+20 35 29.7	7.27	0.581	21.32	0.83	132.60	−581.11	8	4620	-
HD 128167	71284	14 34 40.69	+29 44 41.3	4.47	0.364	64.66	0.72	188.32	132.72	5	360	-
G166-45	72461	14 49 02.36	+25 42 12.2	9.73	0.437	10.28	1.42	−8.94	−346.52	5	8240	SB?
HD 134169	74079	15 08 18.06	+03 55 50.3	7.67	0.565	16.80	1.11	0.71	−14.74	4	3300	-
HD 149996	81461	16 38 17.49	−02 26 29.3	8.50	0.613	14.37	1.18	−177.76	−285.10	3	3600	-
G20-8	86443	17 39 45.81	+02 24 59.0	9.94	0.458	8.35	1.64	−365.79	74.96	6	6100	-
HD 338529	96115	19 32 31.91	+26 23 27.6	9.37	0.390	6.93	1.48	0.91	−172.49	1	3600	-
HD 194598	100792	20 26 11.85	+09 27 05.2	8.33	0.503	17.94	1.24	117.90	−549.71	2	2400	-
HD 201891	104659	21 11 59.11	+17 43 47.8	7.37	0.525	28.26	1.01	−121.58	−898.84	2	1440	-
HD 201889	104660	21 11 59.24	+24 10 04.4	8.06	0.595	17.95	1.44	438.91	109.88	1	1200	-
G41-41	46516	09 29 15.45	+08 38 03.2	11.15	0.390	1.04	2.79	198.54	−307.65	5	11600	-
G48-29	47480	09 40 45.79	+01 01 29.0	10.18	0.405	1.20	8.41	0.23	1.41	4	11700	-
HD 103095	57939	11 52 55.82	+37 43 58.1	6.42	0.754	109.21	0.60	4003.69	−5813.00	1	900	-
G64-12	66673	13 40 02.63	−00 02 18.0	11.47	0.405	3.00	2.40	−230.46	−80.32	8	13850	-
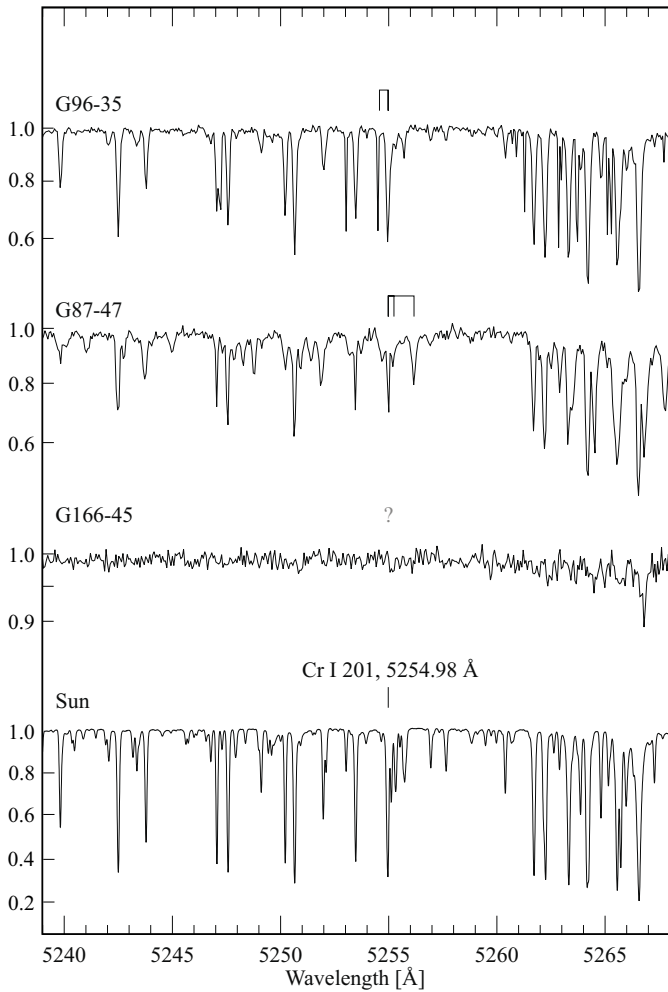
Fig. 2. Double-lined spectra detected in the sample. The components have been marked for the Cr I 201 line at 5254.98 Å. The flux axis is compressed to show approximately the same dynamic range for each star. See text for details

To allow for a comparison with more extremely metal-poor stars, four additional reference stars, observed with the same instrument and resolution, were added.

2.1. Notes on individual stars

It has been mentioned in Paper I that quite a number of the sample stars emerged as spectroscopically *peculiar*, either being spectroscopic binaries or showing Ca II H+K emission cores. The high fraction of binaries among metal-poor stars has also been put forward by Latham et al. (2002) and Fuhrmann (2004) who arrive at a binary fraction very similar to that of normal field stars of the thin disk. Our current list is nearly as contaminated by binaries as was that of Paper I, and we expect that some more binaries would have been detected if the signal and the spectral resolution were increased. Clearly double-lined spectra were detected only for two stars, G96-35 and G87-47. G166-45 could not be fully resolved at our spectral resolution. It is one of the limiting cases where $R = 60000$ would have helped to resolve the asymmetry which was detected near the maximum of a correlation with the solar spec-

trum. In stars such as HD 104800 we detect a systematic line asymmetry probably hiding a secondary component at a velocity difference of only ~ -5 km/s, which could not be resolved with our resolution of 40000. Therefore we have to accept the fact that reliable abundance analyses are possible only for 51 out of 59 stars, and that some of the analyzed single-lined binaries may not represent their binary system adequately. Unlike among the stars of Paper I no strong Ca II emission cores were found in this subsample. In the following some comments are given for the stars that were found spectroscopically peculiar.

G78-1: Known as a single-lined binary (Laird et al. 2002) with a peak-to-peak velocity amplitude of 9 km s^{-1}. Spectrum does not look suspicious

G96-35: Spectrum shows a double-lined system of similar line strengths at $\Delta v = -23.5$ km s^{-1} (see Fig. 2)

G87-47: This spectrum is triple-lined with a strong secondary component at $+68$ km s^{-1} and another weak component which is only partly resolved at $+15$ km s^{-1}. Fig. 2 gives an impression of the complex spectral appearance

G40-8: According to Laird et al. (2002) this is a single-lined binary. The combined spectrum indicates a temperature around 5600 K, and a metal abundance of ~ -0.2

G9-16: Characterized by unusually strong Balmer lines that indicate a temperature significantly above the metal-poor *turnoff*. This star could be a blue straggler.

G58-23: Again, a single-lined binary of Latham et al.'s (2002) table. The spectrum of this star is of roughly solar temperature, and it appears more metal-poor, with [Fe/H] ~ -0.8,

HD 97855A: Visual binary, clearly separated from HD 97855B which itself is a binary

HD 104800: As noted above this star is probably a spectroscopic binary. Its spectrum shows systematically asymmetric absorption lines, which could be the result of a fainter secondary component near a velocity difference of $\Delta v \sim -5$ km s^{-1}

HD 107582: Latham et al. provide a preliminary orbit with a very small velocity amplitude. The spectrum is that of a solar temperature dwarf with [Fe/H] ~ -0.4 and [Mg/Fe] ~ -0.1

HD 108754: Spectroscopic binary (SB1) according to Halbwachs et al. (2003), with a short period of 25 days

G166-45: The star has been identified as an SB2 by Smith, Lambert and Nissen (1998, see also Carney et al. 1994). Our relatively noisy spectra do not allow a final conclusion (see Fig. 2), but the asymmetric velocity correlation function also suggests a spectroscopic binary at the spectral resolution limit.

3. Spectrum synthesis

Model spectra are synthesized from model atmospheres calculated in local thermodynamic equilibrium (LTE). The atmospheric models have been described in a number of papers (Gehren et al. 1991; Fuhrmann et al. 1993). They are plane-parallel and in hydrostatic equilibrium, with convective en-
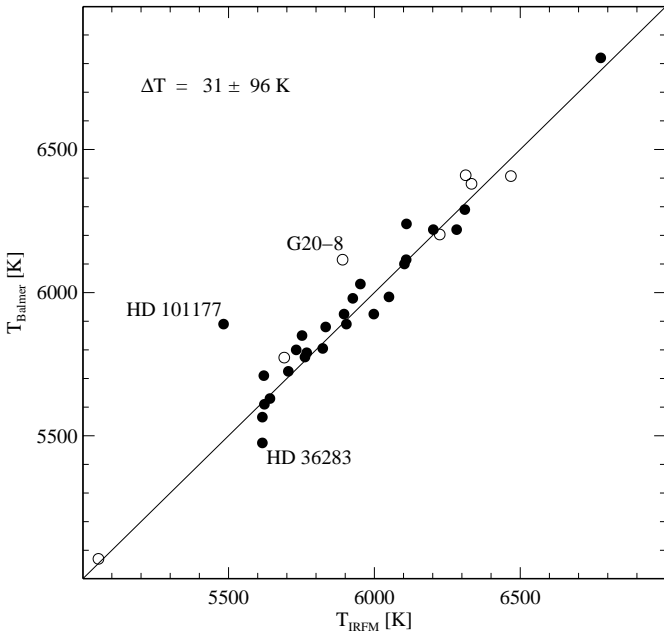
Fig. 3. Comparison of effective temperatures derived from the infrared flux method (Alonso et al. 1996; Blackwell & Lynas-Gray 1997) and from Balmer lines (this paper). Open circles refer to the metal-poor reference stars, filled circles represent the standard sample

ergy transfer calculated from the mixing-length theory as described by Böhm-Vitense (1958) using a mixing-length parameter of $\ell/H_p = 0.5$. Opacities are provided by the most important *bf* absorbers including Rayleigh scattering, and by opacity distribution functions based on Kurucz' (1992) line lists, with a systematic adjustment of the metal abundances of $\log(\text{Fe/H}) = -0.16$ to account for the difference between ODF Fe abundances and a solar value of $\log(\text{Fe/H})_\odot = 7.51$ which is required by fits to theoretical models. With respect to recently calculated hydrostatic models using opacity sampling (see Grupp 2004a,b), the ODF models are identified by a somewhat different temperature scale that accounts for the different temperature stratifications.

3.1. Stellar parameters

Stellar parameters are based on the same methods as in Paper I. Effective temperatures are derived from comparison of model Balmer line profiles (Hα and Hβ) with the observed spectra. For reasons given in Paper I and to remain consistent with the corresponding temperature scale we do *not* apply the self-broadening theory recently put forward by Barklem et al. (2000). Instead we rely on resonance broadening as described by Ali & Griem (1965,1966) and presented in Fuhrmann et al. (1993). Fig. 3 demonstrates that the agreement with infrared flux method temperatures as determined by Alonso et al. (1996) and Blackwell & Lynas-Gray (1997) is satisfactory. The offset between the two temperature scales is 32 K; the r.m.s. error is 96 K.

Surface gravity data are directly obtained using HIPPARCOS parallaxes, together with a reasonable guess of the stellar mass. The latter is uncritical and can be obtained with sufficient accu-

racy from (differential) stellar evolutionary tracks such as those of VandenBerg et al. (2000). The error budget is therefore relatively small with temperature errors mostly between $\Delta T_{\text{eff}} = 50$ and 100 K, and surface gravity errors of $\Delta \log g < 0.05$.

The Fe abundance and the microturbulence are obtained from Fe II lines where no evidence for a deviation from LTE is found. It is clear that for the most extremely metal-poor stars the determination of ξ is more uncertain than for more metal-rich stars. For these stars other lines have also been taken into account. All abundance results except those for Fe II are based on NLTE line formation.

3.2. NLTE line formation

The nature of NLTE effects in the light elements Na, Mg and Al was already discussed in Paper I. It is interesting to note that whereas Na I levels are populated by recombination and collisional decay, both Mg I and Al I are dominated by depopulation due to photoionization. The result of such different ionization processes is most remarkable in some of the extremely metal-poor stars, where the [Al/Na] abundance ratio under LTE and NLTE conditions differs by one order of magnitude.

NLTE line formation calculations have been applied to the present subsample of stars using the same atomic models described in Paper I, except that we took into account the fine structure splitting of the $3p^3P$ term in Mg I, and that of the $3p^2P$ term in Al I. These model variations introduced small systematic changes in the population densities and corresponding abundance determinations of the order of < 0.05 dex, which made us recalculate the stellar subsample from Paper I in order to retain consistent abundance results. The same set of absorption lines (Table 2 of Paper I) was also used to derive single line abundances from profile fits applying either LTE or NLTE population densities.

4. Abundance results

Abundances for the *new* sample stars are shown in Table 2. Not included are stars from Table 1 that show any kind of spectral peculiarity. Due to a degraded S/N below 4000 Å, no Al abundance could be determined for a small number of stars at the faint end.

Table 2 also indicates the maximum errors in surface gravity that propagate from mass, temperature and parallax according to $\Delta \log g = \Delta \log M + 4\Delta \log T_{\text{eff}} + 2\Delta \log \pi$. All values larger than ~ 0.15 dex are essentially determined by a large *parallax* error. We note that even the maximum surface gravity errors do not affect the abundances for neutral metals very much. The reason is that all numerical experiments show $\partial \log \varepsilon / \partial \log g \simeq 0.0 \ldots - 0.4$. The error variation results from line strength; very strong lines such as Mg I 5183 Å in more metal-rich stars show that the strongest influence of the gravity error produces a Mg abundance error of –0.1 dex for a surface gravity error of 0.2 dex. For unsaturated neutral lines the error is almost negligible, and a *mean* abundance error combining the analysis of weak and strong lines will be close to –0.05 dex for a surface gravity error of 0.2.

Eleven stars in Table 2 have maximum surface gravity errors above $\Delta \log g = 0.2$; only three of them are above 0.3. Note that there is a general trend towards uncertain parallaxes with decreasing metal abundances. Statistically, this is easily understood as the result of an increasing space volume. These stars, as well as a number of them in Paper I, do not have strong metal lines; their metal abundances are derived from weak lines that do not depend on surface gravity at all. We also note in passing that an error in surface gravity as large as 0.3 dex is one of the most extreme cases when examining stars near the turnoff.

Another case is the influence on abundance *ratios*, in particular [Na/Mg] or [Al/Mg]. As was outlined above, even the most extreme assumptions about abundance errors due to uncertain parallaxes lead to values around 0.1 dex, where it is most important that such abundance errors of Na, Mg and Al cancel to the per cent level because these elements are all analyzed from their neutral lines. They all have a similar mix of strong (resonance) and subordinate lines which respond to surface gravity variations close to the same amount. As an example, for the very metal-poor star, G41-41, with a parallax error contribution of more than 2 dex, we can safely limit the surface gravity to an error of ± 0.5, i.e. $3.76 < \log g < 4.76$. Within these limits the resulting abundance ratios vary by less than 0.02.

At the per cent level of abundance ratio accuracy the error does not seem to depend very much on gravity determination. This is similar for T_{eff} except for a few stars (e.g. HD 101177, see Fig. 3). The reason is that error progression from T_{eff} tends to cancel to a certain degree for all neutral metals, and the corresponding budgets as well as that of mean microturbulence errors are predominantly systematic for *all* lines of a particular ion in the spectrum of a star.

Our most important errors show up in the standard deviation of single lines. Consequently, using a common microturbulence value the abundances of the subordinate 3p–5s lines in Na I at 6154 and 6160 Å are different from those of the other Na lines already in the Sun (see Baumüller et al. 1998, Table 1). This result could be due to the different influence of hydrodynamic flow patterns, and it may document the limits of plane-parallel abundance analyses. A similar discrepancy occurs between the forbidden Mg I line at 4571 Å and the Mg I *b* triplet at 5172 and 5183 Å. Confirming earlier results, we also find significant NLTE effects for the forbidden transition, but they coincide with similar abundance effects in the *b* lines. In both types of lines such NLTE effects are due to a shift of the line-formation region to deeper and therefore hotter layers resulting from systematic changes in the ionization equilibrium. Aside from hydrodynamical and NLTE influence two other problems are apparent,

– undetected blends may account for part of the scatter, in particular since that scatter would depend in different ways on temperatures and surface gravities, and
– undetected binaries may still be hidden in our list of seemingly "clean" spectra. Assuming a similar binary fraction in metal-poor and metal-rich stars, the number of binaries still remaining as single stars in our investigation could be as high as 50%.
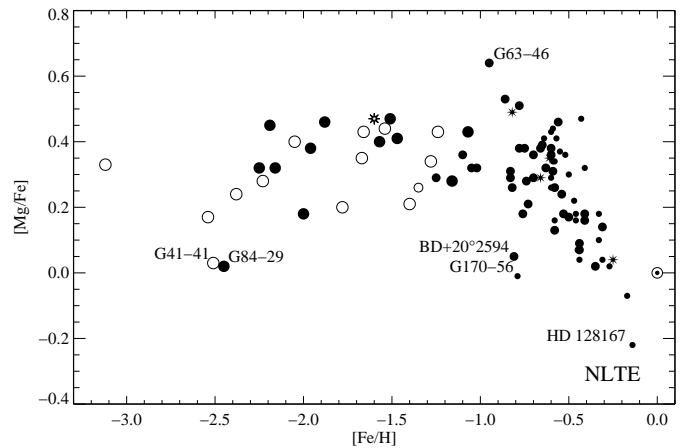

Fig. 4. α-element ratio [Mg/Fe] as a function of metal abundance. Filled circles represent our sample, open circles are the metal-poor reference stars. Symbol size refers to δ(U–B) excesses as in Fig. 1

In LTE the average *internal* errors of single line abundances (*not* the error of the mean) are $\sigma_{\text{[Mg/Fe]}} = 0.050$, $\sigma_{\text{[Na/Fe]}} = 0.046$, and $\sigma_{\text{[Al/Fe]}} = 0.065$. Under NLTE conditions the average single line scatter reduces to values of 0.039, 0.030 and 0.035, respectively. These values are of about the same amplitude as the systematic errors encountered in the determination of the stellar parameters. Total average abundance errors may therefore reach $\Delta \log \varepsilon \simeq 0.10$, whereas the abundance ratios should be even more accurate.

4.1. Mg abundances

Mg/Fe ratios are displayed in Fig. 4. They reproduce the trend seen in earlier investigations of α-element abundances (see Fuhrmann 1998, 2004; Caretta et al. 2000) including significant scatter at the extremely metal-poor end found by McWilliam et al. (1995). At variance with such a large scatter are the recent results of Arnone et al. (2005). They claim to find evidence for very efficient mixing in the early Galactic interstellar medium resulting in halo Mg/Fe ratios with a negligible scatter for all stars of their sample. We note here that their results are incompatible with our analyses for the seven stars in common with our sample. The differences between our and their stellar parameters are systematic, with $\Delta T_{\text{eff}} = 135 \pm 59$ K, $\Delta \log g = 0.31 \pm 0.25$, and $\Delta \xi = 0.43 \pm 0.37$ km/s. This explains much of their systematically *low* iron abundances. The [Mg/Fe] abundance of our common subsample (determined with LTE for comparison) is 0.10 ± 0.16, i.e. a scatter nearly three times as large as in the subsample of Arnone et al. (0.30 ± 0.06). Generally, Mg/Fe NLTE abundance ratios are different from but not more homogeneous than in LTE. The full spread of NLTE [Mg/Fe] abundance ratios of the metal-poor stars, measured for [Fe/H] < -1.0, is $\sigma_{\text{[Mg/Fe]}} = 0.12$, definitely *larger* than expected from the error estimate of the analysis itself.

There are quite a few outliers in Fig. 4, with G63-46 representing the upper limit of the Mg/Fe ratio in the sample. According to its kinematics this could be either a thick disk or a halo star. At the other end we find two other stars, G170-56 and BD+20°2594 with [Mg/Fe] abundance ratios near to

Table 2. Stellar parameters and final abundances of the new program stars including 4 more extreme metal-poor reference stars. ξ is the microturbulence, n denotes the number of spectral lines analyzed. $\Delta \log g$ is the maximum surface gravity error emerging from errors in temperatures, masses and parallaxes (see text)

	Star	$T_{\rm eff}$ (K)	$\log g$	$\Delta \log g$	[Fe/H]	ξ (km/s)	[Mg/Fe] LTE	NLTE	n	[Na/Fe] LTE	NLTE	n	[Al/Fe] LTE	NLTE	n
1	HD 17948	6325.	4.13	0.06	−0.35	1.9	−0.04	0.02	(7)	0.12	−0.00	(6)	−0.15	0.14	(7)
2	HD 19445	5985.	4.39	0.08	−1.96	1.5	0.26	0.38	(5)	−0.11	−0.37	(2)			
3	HD 22309	5900.	4.29	0.09	−0.31	1.3	−0.01	0.04	(6)	0.07	0.00	(6)	−0.03	0.16	(7)
4	HD 22879	5775.	4.26	0.07	−0.83	1.1	0.23	0.31	(6)	0.04	−0.01	(5)	0.16	0.52	(6)
5	HD 30649	5765.	4.26	0.08	−0.58	1.3	0.27	0.34	(6)	0.14	0.05	(6)	0.20	0.45	(2)
6	G84-29	6240.	4.14	0.28	−2.45	1.6	−0.07	0.02	(4)	−0.50	−0.72	(2)			
7	HD 241253	5850.	4.25	0.19	−1.05	1.2	0.23	0.32	(6)	0.01	−0.05	(4)	−0.10	0.30	(3)
8	HD 243357	5675.	4.38	0.19	−0.59	1.1	0.26	0.31	(7)	0.14	0.08	(6)	0.19	0.40	(6)
9	HD 36283	5475.	4.28	0.11	−0.41	0.8	0.27	0.32	(7)	0.17	0.11	(6)	0.28	0.40	(7)
10	G99-21	5525.	4.30	0.30	−0.63	1.0	0.26	0.32	(7)	0.17	0.10	(6)	0.18	0.38	(6)
11	HD 250792	5600.	4.32	0.19	−1.02	1.1	0.24	0.32	(6)	−0.04	−0.13	(4)	−0.36	0.15	(1)
12	HD 46341	5880.	4.36	0.10	−0.58	1.8	0.22	0.26	(7)	0.06	0.12	(6)	0.19	0.31	(6)
13	HD 56513	5630.	4.53	0.09	−0.45	1.2	0.03	0.07	(6)	0.06	0.01	(6)	0.03	0.21	(6)
14	HD 58551	6190.	4.23	0.07	−0.53	1.8	0.12	0.18	(6)	0.07	−0.03	(6)	−0.05	0.25	(6)
15	HD 59374	5840.	4.37	0.12	−0.83	1.4	0.23	0.29	(6)	0.04	−0.03	(5)	0.09	0.35	(5)
16	HD 59984	5925.	3.94	0.07	−0.74	1.2	0.18	0.28	(6)	0.06	−0.01	(6)	0.03	0.41	(5)
17	HD 60319	5875.	4.17	0.14	−0.82	1.4	0.18	0.26	(7)	0.08	0.01	(5)	0.02	0.37	(5)
18	HD 69611	5725.	4.12	0.10	−0.65	1.3	0.31	0.39	(6)	0.18	0.07	(6)	0.23	0.54	(2)
19	HD 233511	6015.	4.29	0.17	−1.57	1.4	0.29	0.40	(6)	0.00	−0.28	(2)	−0.62	−0.11	(1)
20	G9-16	6820.	4.11	0.23	−1.47	2.2	0.39	0.41	(4)	0.22	−0.13	(4)	−0.55	0.11	(1)
21	G235-45	5500.	4.25	0.23	−0.59	1.1	0.38	0.44	(6)	0.21	0.16	(6)	0.19	0.37	(7)
22	HD 84937	6346.	4.00	0.12	−2.16	1.8	0.24	0.32	(4)	0.33	−0.18	(2)			
23	HD 88446	5915.	4.03	0.11	−0.44	1.6	0.02	0.09	(7)	−0.00	−0.09	(6)	−0.08	0.17	(5)
24	HD 88725	5665.	4.35	0.08	−0.70	1.2	0.30	0.36	(6)	0.18	0.12	(6)	0.23	0.51	(7)
25	HD 91784	5890.	4.47	0.13	−0.33	1.3	0.13	0.18	(7)	0.10	0.02	(6)	−0.04	0.18	(6)
26	G119-32	5715.	4.39	0.19	−1.88	1.2	0.34	0.46	(5)	−0.17	−0.46	(2)	−0.32	0.10	(1)
27	HD 94028	5925.	4.19	0.10	−1.51	1.5	0.35	0.47	(6)	0.02	−0.16	(4)			
28	HD 96094	5900.	4.01	0.10	−0.46	1.7	0.11	0.18	(7)	0.05	−0.02	(6)	0.06	0.35	(6)
29	HD 97855A	6240.	4.13	0.09	−0.44	1.8	0.01	0.07	(7)	0.11	0.02	(6)	−0.16	0.15	(6)
30	BD+20°2594	5900.	4.30	0.20	−0.81	1.4	−0.03	0.05	(6)	−0.12	−0.28	(2)	−0.75	−0.23	(1)
31	HD 101177	5890.	4.30	0.07	−0.47	1.8	0.17	0.22	(7)	0.23	0.17	(6)	0.23	0.41	(2)
32	HD 104056	5875.	4.31	0.13	−0.41	1.3	0.09	0.16	(7)	0.13	0.06	(6)	−0.02	0.21	(6)
33	HD 107582	5565.	4.34	0.08	−0.61	1.0	0.30	0.35	(7)	0.11	0.05	(6)	0.17	0.39	(6)
34	HD 108076	5725.	4.44	0.07	−0.73	1.2	0.14	0.21	(7)	0.03	−0.03	(6)	0.07	0.34	(6)
35	HD 110897	5800.	4.34	0.06	−0.58	1.2	0.09	0.16	(7)	0.02	−0.06	(6)	0.04	0.29	(2)
36	HD 114606	5610.	4.28	0.11	−0.57	1.2	0.34	0.41	(6)	0.16	0.09	(6)	0.26	0.47	(7)
37	HD 114762	5890.	4.14	0.10	−0.70	1.3	0.21	0.29	(7)	0.17	0.07	(6)	0.06	0.43	(1)
38	HD 118659	5510.	4.36	0.10	−0.60	1.0	0.33	0.38	(7)	0.20	0.13	(6)	0.24	0.42	(7)
39	G63-46	5725.	3.88	0.25	−0.95	1.2	0.53	0.64	(7)	0.37	0.24	(6)	0.35	0.83	(1)
40	HD 119288	6420.	4.13	0.07	−0.17	1.9	−0.12	−0.07	(6)	0.03	−0.12	(4)	−0.20	0.09	(7)
41	G165-39	6220.	3.96	0.30	−2.00	1.9	0.09	0.18	(4)	0.04	−0.48	(2)	−0.92	−0.16	(1)
42	HD 123710	5790.	4.41	0.07	−0.54	1.4	0.19	0.24	(7)	0.17	0.10	(6)	0.07	0.30	(7)
43	HD 126512	5825.	4.02	0.08	−0.64	1.6	0.34	0.41	(7)	0.19	0.08	(6)	0.24	0.53	(6)
44	HD 128167	6610.	4.29	0.05	−0.14	1.3	−0.25	−0.22	(7)	−0.04	−0.13	(6)	−0.46	−0.10	(5)
45	HD 134169	5930.	3.98	0.10	−0.86	1.8	0.43	0.53	(6)	0.23	0.14	(6)	0.14	0.54	(5)
46	HD 149996	5665.	4.09	0.12	−0.52	1.2	0.30	0.36	(7)	0.20	0.12	(6)	0.19	0.40	(7)
47	G20-8	6115.	4.20	0.22	−2.19	1.5	0.36	0.45	(4)	0.28	−0.25	(2)	−0.90	−0.15	(1)
48	HD 338529	6280.	3.93	0.23	−2.25	2.0	0.21	0.32	(4)	−0.07	−0.44	(2)			
49	HD 194598	5980.	4.27	0.11	−1.16	1.6	0.16	0.28	(6)	−0.00	−0.14	(4)			
50	HD 201891	5900.	4.22	0.08	−1.07	1.2	0.32	0.43	(5)	0.21	0.07	(5)	0.24	0.59	(1)
51	HD 201889	5710.	4.05	0.12	−0.78	1.1	0.42	0.51	(7)	0.25	0.12	(6)	0.24	0.59	(1)
52	G41-41	6380.	4.26	2.37	−2.51	2.2	−0.15	0.03	(4)	−0.62	−0.72	(2)	−1.13	−0.53	(1)
53	G48-29	6410.	4.27	6.13	−2.54	2.3	0.01	0.17	(4)	−0.44	−0.55	(2)	−1.06	−0.45	(1)
54	HD 103095	5070.	4.69	0.06	−1.35	1.0	0.23	0.26	(7)	−0.22	−0.23	(6)	−0.04	−0.04	(6)
55	G64-12	6407.	4.20	0.74	−3.12	2.3	0.14	0.33	(4)	−0.24	−0.32	(2)			

Fig. 6. Element ratio [Al/Mg] as a function of the ratio [Mg/Fe]. Note the separation between the Al-rich and the Al-poor stars at [Al/Mg] = −0.1

Fig. 5. Element ratios [Na/Mg] (top) and [Al/Mg] (bottom) as a function of the metal abundance [Fe/H]. Symbols have the same meaning as in Fig. 4

Unfortunately, a more comprehensive abundance analysis by Cohen et al. (2004) does not list Na abundances.

The [Al/Mg] ratio instead shows a clear separation near a metal abundance of [Fe/H] $\simeq$ −1.1 and an abundance ratio of [Al/Mg] $\simeq$ −0.1. These dividing lines were already detected (with slightly different abundance values) in Fig. 13 of Paper I, where only a much smaller subsample could be analyzed. Disregarding HD 29907 which according to Lindgren & Ardeberg (1996) is a single-lined binary, a few remarks are appropriate:

– the more metal-rich section of the data seems to cluster near values of [Al/Mg] $\simeq$ +0.1. There may exist a very weak trend of a decreasing Al/Mg ratio among these stars towards solar values, in particular if the Sun represents thin disk ratios. However, the scatter in abundance ratios there is $\simeq$ 0.06, not much less than the trend itself.
– the metal-poor stars with [Fe/H] < −1.0 cluster around a mean value of [Al/Mg] $\simeq$ −0.5, however with a scatter about twice as large as that of the disk stars. The latter does not allow to detect any abundance trend *within* this stellar component.
– in between there is a small number of stars with peculiar abundance ratios, among them HD 250792, BD+20°2594, and G170-56. As mentioned in Sect. 4.1, there are no hidden error sources, and the abundance ratios must be considered as real. This is particularly interesting for the latter two stars that were found to have [Mg/Fe] ~ 0.

The Al abundance ratio is even more clearly represented in Fig. 6. Here, the spread of the Mg/Fe ratios found in Fig. 4 among the metal-poor stars no longer spoils the separation between what has originally been named *halo* stars and the less metal-poor rest of our sample. To separate the two subsamples we no longer have to consider the overall metal abundance [Fe/H] (as in the case of Fig. 5).

or even below zero. These stars both differ significantly from the rest of the disk stars by their kinematics (see below). At lower metallicities similar Mg/Fe ratios are found for G41-41 and G84-29, two halo *turnoff* stars with very nearly the same stellar parameters. As was discussed above there is no room for large errors in the abundance ratios. However, whether these stars are genuinely anomalous or only at the outer wings of an otherwise normal abundance distribution remains uncertain.

4.2. Na and Al abundance ratios

Fig. 5 shows the abundance ratios [Na/Mg] and [Al/Mg] as functions of the metal abundance. Both panels display very different relations. The [Na/Mg] ratio seems to document a smooth continuous enrichment of the sodium abundance. Its overall scatter is significantly *smaller* than that of [Mg/Fe], which may reflect a relatively tight coupling of the Mg and Na synthesis. The two outliers are HD 74000, a star being notoriously peculiar (see Beveridge & Sneden 1994), and G119-32, a subdwarf with an extreme retrograde orbit. The most extremely metal-poor stars found to date, HE 0107-5240 (Christlieb et al. 2004) and HE 1327-2326 (Frebel et al. 2005) have been reported to host LTE Na abundances as high as [Na/Mg] $\simeq$ 0.66 and 0.4, respectively, values that are fully outside our relation.
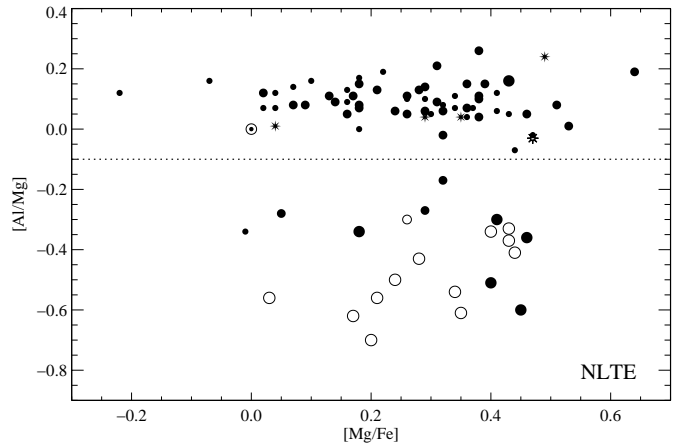
4.3. Comparison with other abundance work

Except for the work of Baumüller & Gehren (1997), Baumüller et al. (1998), and Zhao & Gehren (2000) there are no systematic analyses of Na, Al and Mg including a full account of NLTE line formation for metal-poor unevolved stars. Therefore no direct comparison of our results is possible. However, there are a number of abundance analyses that are carried out under the LTE assumption. Some of them have used NLTE corrections such as those published in the above papers. Whereas these corrections generally give a raw account of the difference between thermal and non-thermal ionization and excitation, they depend on the precise determination of all stellar parameters. Individual corrections treated in such a global way will therefore produce additional abundance scatter in any stellar sample, which may then hide properties of the correlations between the abundance ratios. This is shown in Fig. 7, which demonstrates that NLTE corrections – although following a general abundance trend – can vary strongly with individual stellar parameters.

Of course, the main result is the strong increase with decreasing metal abundance of NLTE Al abundances with respect to LTE, and the simultaneous decrease of the NLTE Na abundances. As stated in Paper I, these large NLTE corrections make LTE abundance analyses of both Na and Al nearly useless for an investigation of Galactic chemical evolution. This is an important limitation for LTE analyses, at least for stars with metal anbundances less than [Fe/H] < −1.5.

In a recent paper Jonsell et al. (2005) have published abundances for a number of metal-poor stars. Their analysis is in LTE, and their abundances are correspondingly different from those reported here. They claim that NLTE corrections for the Na I 5682/5688 doublet are small enough to be neglected. In fact, the corrections are around –0.1 for mildly metal-poor stars, and they even *decrease* with decreasing metal abundance. However, the equivalent widths decrease as well, and the cited abundance values for HD 84937, HD 140283 or similarly metal-poor stars refer to $W_\lambda \leq 5$ mÅ. Our VLT spectrum of HD 140283 which has S/N > 350, and which is probably not worse than that of Jonsell et al., shows only a marginal sign of this doublet with equivalent widths of ∼ 0.7 and 2.5 mÅ, respectively. In a spectral region such as $\lambda \simeq 5700$ Å measurement of equivalent widths is very uncertain because of some unidentified continuum depression encountered there. On the other hand, our present NLTE calculations fit to the 5682/5688 doublet *and* the D lines simultaneously, whenever both can be measured, with a scatter usually below 0.03. Therefore a systematic difference of $\simeq 0.2$ dex is found between their and our metal-poor stars' Na abundances.

A similar discrepancy is found for our respective Al abundances. Since Jonsell et al. claim to have determined their abundances from the Al I 6696/6698 doublet, it is important how possible errors for stars as metal-poor as HD 94028 are handled. We have taken a number of spectra of that star with a combined S/N of more than 300, and we do not find a feature with an equivalent width $W_\lambda > 2$ mÅ at the predicted position. The results presented by Jonsell et al. (2005), however, imply $W_\lambda > 6$ mÅ for the 6696 Å line. In that spectral region, there
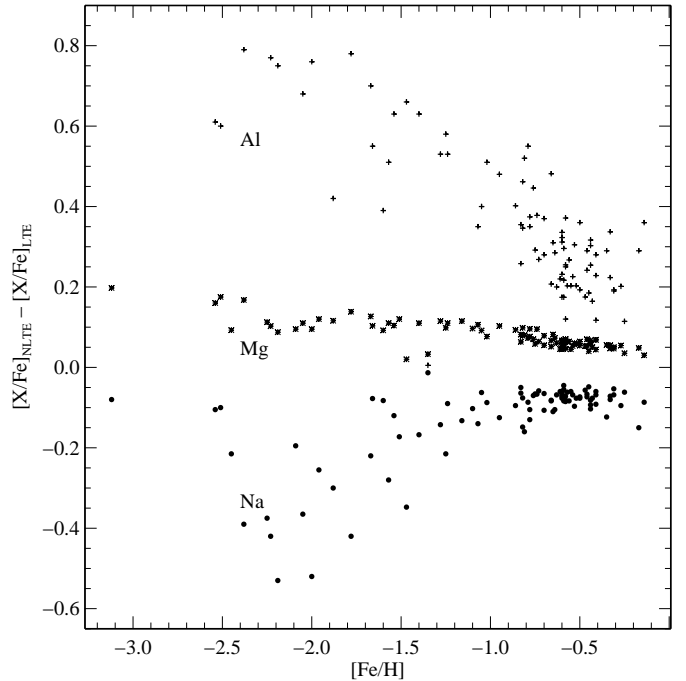

Fig. 7. Difference of element abundance ratios calculated under NLTE and LTE assumptions, respectively

are many faint unidentified lines, most of them probably atmospheric. Also, the RCA chips used in Jonsell's analysis were known for their strong interference patterns which could not be fully removed by flatfield calibration. This may have worked together to suggest a higher continuum position as would be set on account of the photon noise alone.

On the other hand, our NLTE Al abundances that could be determined simultaneously for up to 7 lines including the resonance line, reduced the scatter of the single line abundances by factors of two or three. The often reiterated statement that the uncertainty of collisional cross-sections determines the NLTE results, is simply wrong. There is quite a number of elements such as Na or Si that do not seem to depend on collisions very much at all. Even photoionization-dominated elements such as Mg or Al are *not* very sensitive to variations of the bound-bound hydrogen collision factors[2], as we confirmed when experimenting with new atomic models. As an example Table 3 lists the corresponding changes in the [X/Fe] ratios when varying S_H from 0.001 to 1.0 for a typical metal-poor *turnoff* star, similar to our model of G165-39. We used the observed spectra of this star to perform these calculations which were restricted to the strong lines in the spectrum, because weaker lines are hardly observed in very metal-poor stars. Note the extreme abundance differences for Na and Al with respect to LTE, which is only approached with very high values of S_H ($S_H \gg 1$).

Iron seems to be particularly sensitive to the choice of S_H, due to reasons that are not yet well understood (Korn, Shi & Gehren 2003; Shchukina, Trujillo Bueno & Asplund 2005),

---

[2] The collision factor S_H is defined as a scaling parameter applied to Drawin's (1968,1969) formula for hydrogen collision rates

Table 3. Abundance ratios [X/Fe] for varying collision parameter S_H compared with LTE results for a typical turnoff star, where X represents the elements Na, Mg and Al. All abundance ratios refer to abundances calculated for the spectra of G165-39.

Ion	Line	$S_H = 0.001$	0.01	0.1	1.0	LTE
Na I	5889 Å	−0.44	−0.44	−0.43	−0.33	0.04
Mg I	5184 Å	0.06	0.06	0.07	0.07	0.07
Al I	3961 Å	−0.21	−0.21	−0.21	−0.26	−1.05

and at present it is not possible to model the excitation equilibrium of Fe I very well.

5. Discussion

It was mentioned above that one of the most important goals of our project is the detection of the population membership for *individual* stars. The basic question, if the *stellar population* is still a reasonable concept in view of highly complex merging scenarios, cannot be answered that simply. It may help to find out if it can keep its old meaning or eventually has to take on a new one. Although population originally described stellar kinematics, and correlations with element abundances entered the scene only later, it seems very clear now that both properties contribute to the notion of such words as "halo" or "thick disk". A third stellar property, the evolutionary age, was introduced to the discussion of stellar populations by Fuhrmann (1998), who claimed to have separated the thin and thick disk populations with the help of abundance ratios [Mg/Fe], kinematics (mostly the asymmetric drift velocity), and the age derived from a differential application of modern evolutionary grid calculations.

A more comprehensive study of the problem has been published recently by Bensby et al. (2005). Since their results were obtained with LTE, the abundance ratios for a number of elements are not significant on an absolute scale, but they appear to confirm Fuhrmann's results on a differential scale for a number of other elements.

This paper shows how such a discrimination can be found between *halo* and *thick disk* stars. Starting with the abundance ratios, Figs. 5 and 6 already suggest that the Al/Mg ratios provide the means for a clear separation between halo and (thick or thin) disk stars. For a first approximation, Fig. 6 is divided into two regions with a cut at [Al/Mg] = −0.1. In this paper, all stars below that limit are tentatively assigned the label "halo", and the rest is named "disk" stars bearing in mind that this type of classification requires confirmation from stellar kinematics and ages.

5.1. Kinematics

Table 4 presents the kinematic data for the new stars observed. They will be supplemented here by the data of Paper I. Some of the radial velocities have been redetermined from our spectra. The *Local Standard of Rest* velocities refer to a solar motion of $(U, V, W)_\odot = (10.1, 4.0, 6.7)$ km s^{-1} (see Hogg et al. 2005).
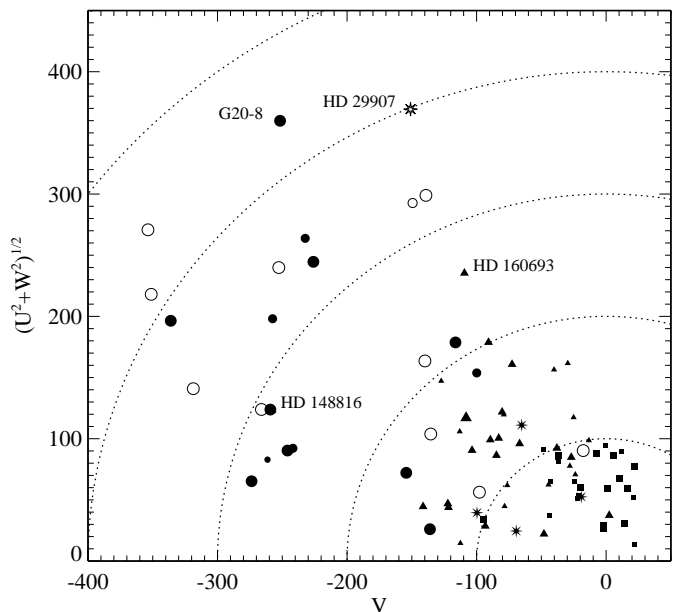

Fig. 8. Galactic space velocities of the stellar sample. Open symbols refer to the extremely metal-poor reference sample, filled symbols to the metal-poor standard sample. Circles follow the requirement [Al/Mg] < −0.10, triangles require [Al/Mg] > −0.10, but [Mg/Fe] > 0.25, and squares represent stars with [Mg/Fe] < 0.25. Star symbols denote peculiar objects as defined in Table 1

Except for a few stars, the program stars have reliable parallaxes with HIPPARCOS measurements resulting in $\sigma_\pi/\pi < 0.25$. The stars with higher parallax errors are G84-29, G99-21, and G165-39, all with $\sigma_\pi/\pi < 0.30$, and the more extreme stars of the reference sample G41-41, G48-29, and G64-12 with fractional errors of between 0.65 and 1.50. Because of significant parallax error propagation into transversal space velocities these stars are excluded from the kinematic analysis. The corresponding space velocities of these stars (Comments 1 or 2 in Table 4) may be in error by large amounts.

It was mentioned before in many publications, that stellar kinematics can only lead to a *statistical* description of the Galactic populations. This is also evident for our sample, demonstrated in the Toomre diagram (Fig. 8) as clearly as in Fig. 9, where the asymmetric drift velocities are plotted against the [Al/Mg] abundance ratios. Similar to kinematic properties of the thick disk (see Fuhrmann 2004), there exists a substantial overlap between the "halo" and the thick disk. We find high-velocity thick-disk stars such as HD 148816 and HD 160693 at total space velocities that are generally reserved for halo stars. In fact, HD 148816 is kinematically extreme in that it even follows a *retrograde* Galactic orbit. On the other hand, a number of halo stars with very low space velocities are found, among them HD 31128 and HD 97320. Since we had to disregard the extreme stars with uncertain parallaxes, the maximal space velocity of our sample is near $V_{LSR} = 440$ km s^{-1} (HD 74000, G20-8).

The distribution of the asymmetric drift velocities is seen best in abundance plots such as Fig. 9. Here, the stars with low space velocities appear as the positive tail of a halo velocity distribution centered near $V = −220$ km s^{-1}. It is also easy

Table 4. Kinematic results, ages and classification of metal-poor stars analyzed in this paper. Columns (3) to (7) are in km/s, Col (9) is in solar masses, and (10) in Gyr. Classification in terms of population membership refers to abundances ratios (left), kinematic properties (middle), and ages (right). The following notation is used: D: thin disk ([Al/Mg] > −0.1 and [Mg/Fe] < 0.25, V > −40 km s^{-1}, age < 10 Gyrs) T: thick disk ([Al/Mg] > −0.1 and [Mg/Fe] > 0.25, −120 < V < −20 km s^{-1}, age > 10 Gyrs), and H: halo ([Al/Mg] < −0.1, V < −50 km s^{-1}, age > 10 Gyrs). Whenever parallax errors are > 25% masses and ages have not been determined because of uncertain absolute magnitudes

	Name	V_{rad}	U	V	W	V_{LSR}	M_{bol}	Mass	Age		Class		Comment
1	HD 17948	28.0	−20.0	11.6	19.6	30.3	3.35			D	D		age fit failed
2	HD 19445	−139.0	168.0	−116.3	−60.9	213.2	4.92	0.64	27.4	H	H,T	H,T	
3	HD 22309	−27.0	76.5	−2.0	−51.9	92.4	4.24	0.94	10.1	D	D	H,T	
4	HD 22879	115.0	−94.3	−82.9	−34.6	130.3	4.59	0.78	18.7	T	D,T	H,T	
5	HD 30649	25.0	−44.7	−78.4	−2.7	90.3	4.42	0.88	14.1	T	H,T	H,T	
6	G84-29	177.0	−123.1	-166.3	-29.2	209.0	4.07				H		σ_π/π = 0.27, no Al
7	HD 241253	−16.0	22.3	−89.4	96.6	133.5	4.59	0.74	20.4	T	H,T	H,T	
8	HD 243357	−19.0	21.5	−93.3	18.8	97.5	4.93	0.83	14.3	T	H,T	H,T	
9	HD 36283	49.0	−13.9	−76.3	−60.3	98.2	4.78	0.82	21.4	T	H,T	H,T	
10	G99-21	134.0	-52.0	−228.4	31.7	236.4	4.76			T	H		σ_π/π = 0.29
11	HD 250792	−186.0	244.7	−232.3	98.5	351.5	4.95	0.66	30.6	H	H	H,T	
12	HD 46341	8.0	16.0	−29.9	70.6	78.3	4.60	0.89	10.2	T	D	H,T	
13	HD 56513	−31.0	50.3	−22.8	11.1	56.3	5.12	0.81	13.2	D	D	H,T	
14	HD 58551	51.0	−52.9	−1.5	−20.0	56.6	3.97	1.02	6.2	D	D	D	
15	HD 59374	92.0	−46.9	−122.2	0.0	130.9	4.85	0.80	13.5	T	H	H,T	
16	HD 59984	56.0	−19.0	−48.0	−11.3	52.8	3.40	1.00	8.2	T	T	D	
17	HD 60319	−37.0	72.5	−84.7	−47.0	121.0	4.21	0.82	15.2	T	H,T	H,T	
18	HD 69611	113.0	−25.5	−141.3	−36.5	148.1	4.12	0.90	14.0	T	H	H,T	
19	HD 233511	61.0	−120.4	−259.2	28.8	287.2	4.57	0.69	22.0	H	H	H,T	
20	G9-16	58.0	−35.4	−246.0	−83.1	262.0	3.27			H	H		age fit failed
21	HD 84937	−24.0	244.5	−226.0	−6.9	333.0	3.59	0.74	15.5	H	H	H,T	no Al abundance
22	G235-45	−33.0	−119.8	−127.3	−85.5	194.6	4.80	0.81	22.2	T	H	H,T	
23	HD 88446	60.0	−30.6	−97.3	7.4	102.3	3.56	1.01	8.5	D	H,T	D	
24	HD 88725	−24.0	83.1	−26.9	−16.8	89.0	4.76	0.80	19.1	T	D,T	H,T	
25	HD 91784	−30.0	77.4	−38.5	−19.2	88.5	4.75	1.01	2.4	D	D,T	D	
26	G119-32	74.0	171.9	−336.1	95.0	389.2	5.14	0.55	11.0	H	H	H,T	
27	HD 94028	62.0	−21.6	−136.0	14.5	138.5	4.45	0.70	23.3		H	H,T	no Al abundance
28	HD 96094	1.0	−80.8	−50.1	−39.0	102.7	3.63	1.01	8.6	D	H,T	D	
29	HD 97855A	−41.0	52.1	14.2	−21.6	58.2	3.45			D	D		age fit failed
30	BD+20°2594	98.0	−91.2	−241.8	13.1	258.8	4.48	0.77	17.5	H	H	H,T	
31	HD 101177	−17.5	−41.0	−24.1	−28.0	55.2	4.48	0.93	9.7	D	D,T	D	
32	HD 104056	−23.0	76.0	−10.1	−38.7	85.9	4.38	0.93	10.5	D	D	H,T	
33	HD 107582	−82.0	8.7	−99.7	−38.5	107.2	5.01	0.79	19.7	T	H,T	H,T	
34	HD 108076	−3.0	−83.1	−39.4	−9.1	92.4	5.03	0.78	14.9	D	D,T	H,T	
35	HD 110897	80.0	−31.6	10.2	81.7	88.2	4.59	0.83	14.8	D	D	H,T	
36	HD 114606	27.0	−147.0	−29.6	67.3	164.4	4.65	0.84	18.0	T	D,T	H,T	
37	HD 114762	49.0	−71.6	−66.8	63.9	116.9	4.11	0.88	12.7	T	H,T	H,T	
38	HD 118659	−46.0	73.6	−38.0	−55.7	99.8	5.03	0.78	21.5	T	D,T	H,T	
39	G63-46	−26.0	161.0	−90.8	−77.7	200.5	3.57	0.98	9.7	T	H,T	D	
40	HD 119288	−15.0	-35.3	−45.5	0.6	57.6	3.29			D	D		age fit failed
41	G165-39	−167.0	304.4	−260.8	−137.9	423.9	3.52			H	H		σ_π/π = 0.30
42	HD 123710	7.0	−25.5	−4.2	7.0	26.7	4.83	0.88	9.9	D	D	D	
43	HD 126512	−53.0	96.5	−79.0	−70.8	143.5	3.75	0.99	10.0	T	H,T	H,T	
44	HD 128167	0.2	11.9	20.0	1.5	23.3	3.42			D	D		age fit failed
45	HD 134169	25.0	28.5	2.4	24.1	37.4	3.68	0.98	9.54	T	D	D	
46	HD 149996	−42.0	3.4	−112.5	−14.2	113.4	4.10	0.92	13.6	T	H,T	H,T	
57	G20-8	−395.0	−349.5	−251.7	85.8	439.2	4.35	0.66	25.5	H	H	H,T	
48	HD 338529	−128.0	42.7	−154.3	−58.1	170.3	3.37	0.77	14.5		H	H,T	no Al abundance
49	HD 194598	−247.0	−60.7	−273.7	−23.9	281.4	4.45	0.75	18.3		H	H,T	no Al abundance
50	HD 201891	−43.0	104.6	−108.1	−52.5	159.3	4.45	0.79	17.0	T	H,T	H,T	
51	HD 201889	−103.0	−117.9	−80.3	−30.6	145.9	4.14	0.88	14.8	T	H,T	H,T	
52	G41-41	266.1	1107.3	−1251.6	282.5	1694.8	4.13				H		σ_π/π = 2.68
53	G48-29	−59.0	34.7	46.9	-26.1	63.8	4.21				H		σ_π/π = 7.01
54	HD 103095	−98.0	292.6	−149.4	−6.4	328.5	6.31				H	H	D	age fit failed
55	G64-12	442.5	−15.4	−428.9	402.3	588.2	4.11				H		σ_π/π = 0.80, no Al

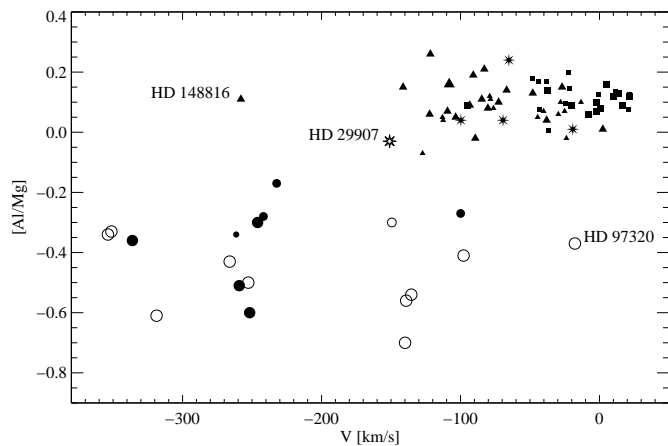**Fig. 9.** Correlation of asymmetric drift velocities and [Al/Mg] abundance ratios. Symbols are the same as in Fig. 8

Fig. 10. Correlation of stellar ages and [Al/Mg] abundance ratios. Symbols are the same as in Fig. 8

to recognize that the overlap of the asymmetric drift velocity distributions of the three Galactic populations is fairly strong. In our admittedly non-representative sample there do not exist clear limits between thin and thick disk. Kinematically, such boundaries do not exist either between thick disk and halo. It is the additional knowledge of the [Al/Mg] abundance ratios that can resolve the overlap in drift velocities. We note that the correlations with the other velocity components U and W are even less conclusive than that with the asymmetric drift.

A few stars do not fit into the picture. Most conspicuous is HD 148816. According to kinematics it would be a clear halo candidate, with a velocity component $W = -71$ km s^{-1} and an asymmetric drift velocity of $= -258$ km s^{-1}. Its abundances, however, are typical for thick-disk stars (see Paper I). It could be important to have a more complete abundance analysis for this star. The problem remains that HD 148816 follows a *retrograde* orbit with only a moderate U velocity. This is not what one would expect for a disk star. The case of HD 97320 is less extreme. Its total space velocity is near 92 km s^{-1}, of which most is due to the U component. HD 29907 is a single-lined binary (Lindgren & Ardeberg 1996), a status that does not explain, why the Al abundance is so high, [Al/Fe] = 0.41. In every other aspect that star would be a halo star.

In Fig. 5 another two stars, BD+20°2594 and G170-56 (see Paper I), were conspicuous with their Fe abundances being substantially higher than expected for halo stars. Though not quite as metal-rich, HD 250792 shows similarly high Fe abundances. According to an [Fe/H] criterion the three stars would rather belong to the thick disk, whereas [Al/Mg] identifies them as halo star candidates. What is more important, all three stars have *retrograde* Galactic orbits, and it seems impossible to relate their membership to a dissipative disk population.

5.2. Stellar ages

Unfortunately, stellar evolution on the main sequence and around the turnoff is still one of the more complicated and therefore uncertain topics of current research. This is so because a number of physical processes cannot be properly addressed. It starts with the α-element abundance ratios, the so-
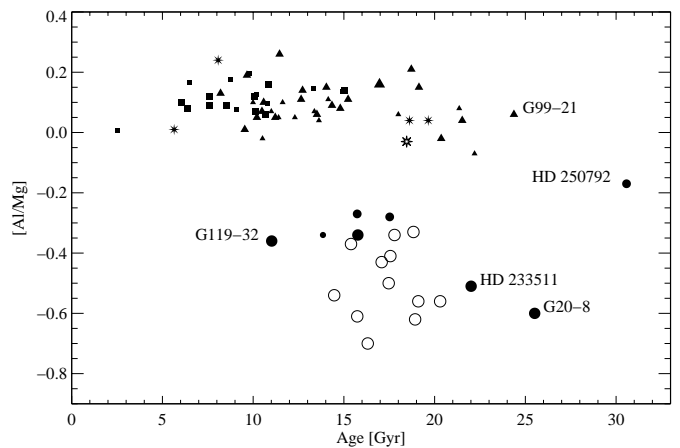
lar value of which has recently been revised by ~ -0.25 dex (Asplund, Grevesse & Sauval 2005). A corresponding change in opacities and mass densities is the result, because all other physical processes have to be normalized to the solar model, which would have to be revised by quite an amount. In turn, such a revision of the solar model is in apparent contradiction to the solar standard model which seemed to be well established by comparison with helioseismology (Bahcall et al. 2005a,b). Another problem is diffusion, a process generally neglected in most of the available stellar model grids. It essentially decreases the time scale of main sequence evolution. It is only realistic to admit that the determination of stellar ages, whether in Globular Clusters or in the field, cannot yet be achieved on an absolute time scale. Instead it may be possible to calculate a set of *differential* ages with a less extreme error estimate. As discussed below for some cases, there exists currently no reliable way to estimate such errors. Whereas masses can perhaps be determined for stars off the main sequence with a differential accuracy better than $\sim 0.05 M_\odot$, the error estimate of stellar ages – even differentially and off the main sequence – depends on both individual stellar parameter error bars and more theoretical insight into the results of metal diffusion.

For our age estimates the same grid of stellar models as in Paper I was used (VandenBerg et al. 2000), where no diffusion is accounted for. Masses and ages from the fits to such evolutionary tracks are given in Cols. (7) and (8) of Table 4. Missing ages document the failure to find a consistent solution by logarithmic interpolation in a set of parameters, T_{eff}, M_{bol}, [Fe/H], and [α/Fe], where the latter was simply replaced by [Mg/Fe]. As is evident from Table 4, some of the stellar ages are beyond 20 Gyr, a completely unrealistic value, both absolute *and* differentially. Of the rest of the sample, most of the halo stars have values above 15 Gyr, still unacceptable in view of the WMAP results that center around an age of the universe of 13.7 Gyr (Spergel et al. 2003). Therefore, the best to be expected is some very coarse *order of ages*. This is given in Fig. 10, and even there the unreasonable spread of halo star ages tells us that there does not exist at present a reliable way to derive stellar ages of metal-poor main sequence or turnoff stars.

The reason for our failure to determine the ages of thick disk and halo stars is not clear at this moment. In fact, there are many ways to produce systematic errors both on the empirical *and* the theoretical side of the problem. We start with the theoretical side, where we have already mentioned above that the problem of the oxygen (and neon) abundances has not been solved (Bahcall et al. 2005a), although there remains the possibility to replace part of the solar oxygen by neon and retain essentially the same solar model (Bahcall et al. 2005b). Of course, a higher solar neon abundance may have a differential effect that could show up in metal-poor stars. The change of the α-element parameter [α/Fe] (previously based on oxygen) due to neon would be –0.1 dex if a decrease of $\Delta \log(\text{O/H}) = -0.2$ were compensated by an increase of $\Delta \log(\text{Ne/H}) = +0.45$. Reducing [$\alpha$/Fe] by 0.1 dex would, however, not change the stellar ages very much.

Larger corrections could instead be achieved by taking into account He diffusion as calculated for metal-poor halo stars by Salaris, Groenewegen & Weiss (2000). It may account for isochrone shifts of up to ∼ 200 K, which is about the necessary adjustment to reduce most of our empirical stellar ages (see Table 4) to acceptable values of, say, 14 Gyr. This is particularly valid for the bulk of the halo stars with ages between 15 and 20 Gyr.

A second diffusion correction is introduced by metal diffusion, i.e. metal nuclei sinking down below the stellar surface with respect to hydrogen. That process is estimated to be particularly efficient for metal-poor stars (Richard et al. 2002a,b), and the effect is supposed to take on a maximum near stars of 0.7 to 0.8 $M_\odot$, i.e. just the mass range most important in our investigation. Thus, halo and thick disk stars are probably all affected, and their present metal abundance may well be associated with an initial value that was ∼ 0.3 dex higher. In that case our age determinations are built on metal abundances that are too low by that amount. Repeating the isochrone fits with more metal-rich mixtures could then again relax the resulting ages by roughly 2 Gyr, although possibly not as much as with the He diffusion. Both effects require improved stellar evolution models taking account of diffusion processes, turbulent phenomena, and radiative acceleration.

On the empirical side, some of the stars with ages above 15 Gyr are extremely sensitive to changes in stellar parameters, in particular effective temperatures and α-element ratios (e.g. [Mg/Fe]). Consequently, some of the extreme *turnoff* stars are reduced to ages of ∼ 14 Gyr, if T_{eff} were *increased* by 200 or 250 K. This would result in roughly the same change of fitting ages as could be achieved by including diffusion in the stellar structure models as discussed above. Our current temperature scale, calibrated with Balmer line profiles, and in accordance with the infrared flux method results, gives no reasonable way to *increase* atmospheric temperatures as would be necessary for the ODF models. Balmer line profile fitting using the original Ali & Griem (1965,1966) approximation to resonance broadening, rather *underestimates* line-broadening processes (see Barklem et al. 2000), and it would emerge into a general decrease of our temperature scale when strengthening the line-broadening processes. Opacity sampling models using a reduced resonance-broadening parameter to fit the solar

Table 5. Definition of population membership for different stellar properties

Population	[Al/Mg]	[Mg/Fe]	V (km s^{-1})	Stellar ages
Thin disk	> −0.10	< 0.25	> −40	< 10 Gyr
Thick disk	> −0.10	> 0.25	< −20	> 10 Gyr
			> −120	
Halo	< −0.10		< −50	> 10 Gyr

Balmer lines, however, require increased effective temperatures for metal-poor turnoff stars (Grupp 2004b).

Absolute magnitudes are mostly reliable, because they are based on HIPPARCOS parallaxes. There are a few exceptions, where parallax errors play a role (see Sect. 5.1), but they are not always identical with the highest ages in Fig. 10. Stars like G119-32 and HD 103095 are so near to their initial main sequence that their ages can be determined only with large error bars. The conclusion is that some of the other stars may still hide an undetected peculiarity. Note also, that uncertain parallaxes affect the surface gravities, although they do not very much affect the abundance ratios (see Sect. 4).

Keeping in mind that the halo stars in Fig. 10 mostly require a *negative* age correction, it seems as if the unmodelled diffusion is responsible for their high ages. It is the single most evident *systematic* error source if the empirical temperature determination is disregarded (see above). But even with appropriate age corrections halo stars could not be separated from thick-disk stars were it not for their different [Al/Mg] abundance ratios. Therefore, stellar ages alone cannot be used for population identification, at least not for individual stars.

5.3. Stellar populations

The wide distribution of the asymmetric drift velocities of halo stars in Fig. 9 proves that kinematic properties of these stars cannot be used for any other but a *statistical* identification of metal-poor stars. For velocities as far off as $V = -100$ km s^{-1} there are thick-disk and halo stars, and for $V = -40$ km s^{-1} all three populations may be co-existent. According to Fig. 10 this may be different for the ages. At least the thin-disk stars seem to be separated from the other two populations. However, as noted in Paper I, our sample of metal-deficient stars does not reproduce the age gap between thin and thick-disk found by Fuhrmann (2004).

To find a reproducible way to address the individual population membership of our stars, single flags have been set for each of the 3 categories, abundance, kinematics, and age. They follow a system of parameters defined in Table 5. Such a set of definitions is always somewhat arbitrary, so it will be used here only as a working hypothesis taking into account very rough boundaries between parameter distributions. Such identification flags are set in columns (11) to (13) of Table 4. We note that the boundaries set for kinematics and age are particularly uncertain.

Analysis of the classification flags including the data of Paper I makes it necessary to remove from the sample all stars

for which one of the three categories could not be measured. This is the result of missing or unreliable data (uncertain parallaxes) or a failure of the age fit due to the limitation of the grid of evolutionary tracks. Out of 92 stars included so far 14 do not provide all parameters. Out of the remaining 78 stars 56 (71.8%) fit into the three categories. They can be assigned a unique population identification with no further investigation. Most of the rest of the sample fits to at least two categories, always including abundances. Whenever one of the categories fails it is important to look for an explanation.

Eleven stars have a discrepant age. Four of them are within 1 Gyr of the boundary. These are all thin-disk stars and need no further investigation because of the uncertainty of both age determination and the setting of a boundary. Two other stars have peculiar abundances. According to their Al/Mg ratio, G63-46 and HD 200580 are of thick-disk type, but their other abundance ratios are [Mg/Fe] = 0.64 and 0.46, and [Al/Fe] = 0.83 and 0.67, respectively. This indicates a strong over-abundance of α-elements only, since [Na/Fe] = 0.24 and 0.36, respectively, is similar to values found in the other thick-disk stars. Two stars, HD 56513 and HD 103095, are so near to their initial main sequence, that their ages are completely unreliable because they vary with very small changes of the stellar parameters. This is a particular problem for HD 103095 and its temperature uncertainty of at least 100 K. Note that we have also assumed that [α/Fe] = [Mg/Fe]. Two of the remaining three stars, HD 108076 and HD 110897, yield ages that are 5 Gyr above the thin-disk boundary. They are relatively sensitive to changes in both $T_{\rm eff}$ and [α/Fe]. Adjusting their ages to the upper limit of the thin-disk requires a temperature correction of $\sim +100$ K. A single star, HD 59984, can not easily be explained. The age defect is similar to that of the high α-element thick-disk stars G63-46 and HD 200580, but both [Mg/Fe] and V of HD 59984 are more near to thin-disk characteristics.

Nine stars have discrepant kinematics. Four of them are within $\sim$ 10 km s^{-1} of the kinematic boundary, and they are probably all thick-disk stars. HD 29907 is a thick-disk star if its Al/Mg ratio is used as a criterion. This may or may not have to do with its companion star, but it could also mean that our Al/Mg boundary is a bit too low. In that case, HD 29907 would be a halo star, in better agreement with the drift velocity of $V = -151.0$ km s^{-1}. HD 69611 is classified as a thick-disk star according to its Al/Mg ratio. Its drift velocity is $V = -141.3$ km s^{-1}, which is low for our definition, but may represent an outlier of the thick-disk population. HD 88446 is more extreme. According to its abundances and age it is undoubtedly a thin-disk star, which is in apparent conflict with its low drift velocity (-97.3 km s^{-1}). A similar case is HD 96094 with $V = -50.1$ km s^{-1}, however, this could still be a thin-disk star. As already discussed in Sect. 5.1, HD 148816 represents a real problem. This is a peculiar star both in terms of its abundances or kinematics. It is hard to believe that retrograde orbits are possible in a disk population, but neither Na/Fe nor Al/Fe are within the abundance distributions of halo stars.

Another two stars are problematic. HD 134169 has high [Mg/Fe] = 0.53 and [Al/Fe] = 0.54, which suggests that it belongs to the thick disk whereas both kinematics and age identify it as a thin-disk star. HD 198300 would also be classified as

a thick-disk star with [Mg/Fe] = 0.29, whereas both kinematics and age would yield a thin-disk result. The Mg/Fe value is very near to the discrimination boundary, thus taking account of the analysis errors it could be at the top of the thin-disk values.

Among the stars with coherent classification criteria, we find the more metal-rich "halo" stars G170-56, HD 250792, and BD+20°2594. With their retrograde orbits, these stars may in fact extend the generally accepted halo star Fe abundances to values as high as [Fe/H] = –0.8 (the so-called metal-rich halo stars). Another explanation would instead identify those stars as members of some accreting process at a very early stage of Galactic evolution (Gratton et al. 2003). However, this would not explain why the stars are much more enriched in iron than the rest of the halo stars. Therefore, we may as well accept them as members of the Galactic halo, which itself could be composed of merging events.

As a result, our classification scheme seems to work well. The [Al/Mg] abundance ratios, together with [Mg/Fe] allow for an immediate identification of nearly 75% of the sample stars. Eliminating the uncertain stellar ages as a population indicator, that number would rise to 87%. Again, reshaping both kinematic and abundance boundaries by a small amount would push the result to 94%. The remaining stars withstand a reasonable identification. They are either peculiar in abundances or kinematics, and they deserve a closer look in future investigations (HD 88446, HD 148816).

5.4. Nucleosynthesis

The abundance ratios of [Na/Mg] and [Al/Mg] have not been discussed in the literature in much detail since the early work on carbon burning nucleosynthesis published by Arnett & Truran (1969) and Truran & Arnett (1971). The resulting yields of typical supernovae seem to depend on the temperature of the exploding shell, the initial C/O ratio after core He burning, and the neutron excess. In a standard scenario today the above parameters are calculated from exploding supernova models on the basis of consistently chosen model characteristics (see Woosley & Weaver 1995). In this environment ^{23}Na results from carbon burning whereas ^{27}Al would be produced during neon burning with only a small fraction coming from carbon burning. In principle, both elements should therefore be *primary*.

However, the yields of ^{23}Na and ^{27}Al are *both* shown to depend on the available neutron excess η prior to the supernova explosion (Woosley & Weaver 1995; Arnett 1996, Chapt. 9). In stellar generations hosting already a significant metal abundance, therefore, ^{23}Na and ^{27}Al should behave more like *secondary* nuclei obtaining at least a fraction of the additional neutrons from stable neutron-rich nuclei that were produced in preceding stellar generations. The smaller the metal mass fraction in the stellar parent generation, the more important becomes the *primary* process based only on ^{12}C produced by He burning. This bimodal scheme was noted already by Arnett (1971) and Woosley & Weaver (1982), and it seems to work in the upper panel of Fig. 11 which reproduces Fig. 5, together with the chemical evolution curve of Timmes et al. (1995). Except
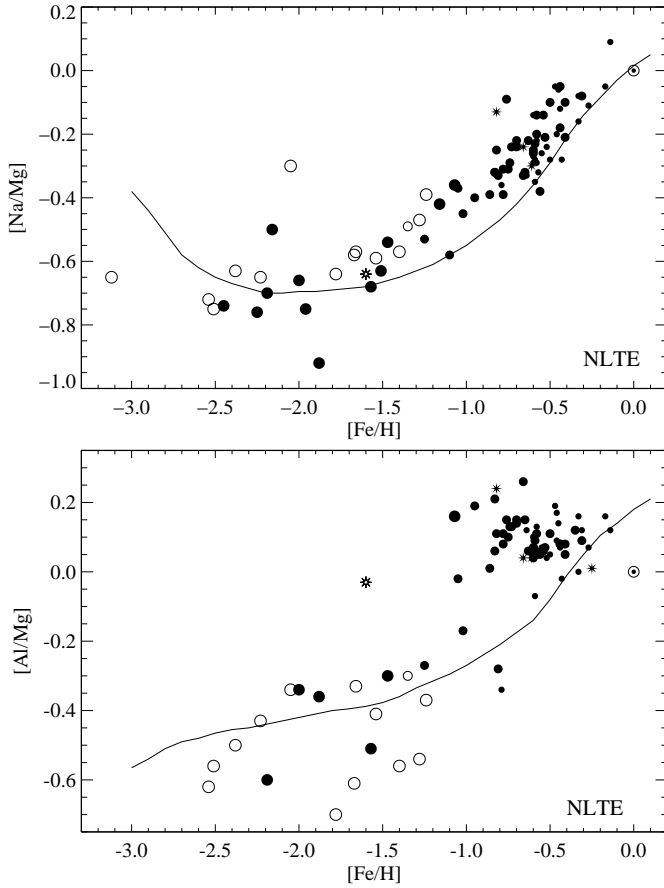
Fig. 11. Galactic evolution of [Na/Mg] and [Al/Mg] abundance ratios. Abundances are the same as in Fig. 5. The theoretical curves are from Timmes et al. (1995)

for the extremely metal-poor tail, for which we have only the evidence from a single star (G64-12), we note a shift of the observed [Na/Mg] with respect to the predicted path of chemical evolution by ~ −0.3 in [Fe/H]. Most of that shift can be eliminated reducing the iron yield by a factor of 2 in the theoretical evolution models (see Figs. 17 and 18 of Timmes et al. 1995). Our [Na/Fe] and [Na/Mg] ratios are then in *full agreement* with the predictions of supernova synthesis provided the mass cut is adjusted as was already proposed by Timmes et al.

Ryan et al. (1996) have addressed the problem for Al, although their data did not allow then to detect anything other than a smooth increase of the [Al/Mg] ratio with [Fe/H], with some flattening of the [Al/Fe] ratio at low metal abundances. Their [Al/Mg] ratios differ from that calculated by Timmes et al. (1995), which were based on the explosion models of Woosley & Weaver (1995). They are, however, in agreement with our results, provided that their Al abundances are corrected for relatively strong NLTE effects. As a result, we find in the lower panel of Fig. 11 a significant discrepancy between theoretical and empirical data, not so much for the extremely metal-poor stars but in particular for stars of the thick and thin disk. We have no doubt that our Al/Mg abundance ratios for these stars are well-determined. *Differential* errors among the abundances should be very small, possibly less than 0.05 dex; therefore the slight increase of the [Al/Mg] ratios towards lower

metal abundances in the disk could be real, although it is statistically not significant. But even if the NLTE corrections were cut in half, the [Al/Mg] ratios would be constant in the disk populations, where Timmes et al. predict a factor of two increase. Taken at face value, this means that in disk stars ^{27}Al is *not* affected by a secondary process.

Why do ^{23}Na and ^{27}Al follow such different enrichment histories? It is obvious that the different behaviour of Na and Al, in particular the primary character of [Al/Mg] in the disk stars, cannot be explained in a simple way. As is already seen from Fig. 6 the two disk populations with 63 stars occupy an abundance level of [Al/Mg] = 0.09 ± 0.06, which must be considered a very small scatter. On the other hand, the 22 extremely metal-poor (halo) stars show a completely different abundance ratio of [Al/Mg] = −0.43 ± 0.14. With our current set of data it cannot be excluded that there is a small trend of [Al/Mg] increasing with [Fe/H] at the metal-poor end as is suggested by the more extreme stars in Ryan et al.'s (1996) sample. That would be as well compatible with the results of Cohen et al. (2004) who instead obtain a slight *decrease* with increasing metal abundance in their most metal-poor stars. Although the scatter among the halo stars is relatively large, it is important to note that here the [Al/Mg] ratio does not vary with [Mg/Fe]. This is the same behaviour as found for the disk populations with the single difference that the Al/Mg ratio in the halo is a factor of three smaller than in the thin or thick disk. Since the distribution of Mg/Fe ratios is similar in halo and (thick) disk populations, the difference must be hidden in the properties of the progenitor stars that produced either of the two abundance ratios.

Tsujimoto et al. (2002) have proposed a scenario in which the [Al/Mg] ratios are produced during *two* generations of SN-induced star formation. There the enrichment of primary nuclei such as ^{24}Mg depends strongly on the first-generation (Pop III) stellar mass, while the [Al/Mg] ratio varies with the mass of the second-generation supernova. The independence of [Al/Mg] could therefore be due to the parent supernovae. Thus halo stars would be *third-generation* long-lived objects that have individual (unmixed) chemical properties with a relatively large scatter of [Al/Mg] ratios. This hypothesis could also explain the [Na/Mg] ratios and their smaller scatter in halo stars, but not the different behaviour of the two elements in stars of the disk populations.

In stars of the thick (and thin) disk the [Na/Mg] ratio is well explained as the result of a secondary process, i.e. the increase of metals that feed additional neutrons into the carbon burning shell. The reason for a nearly constant [Al/Mg] ratio in both disk populations remains to be detected.

6. Conclusions

The results of our spectroscopic investigations of metal-poor stars have brought to light a well-defined criterion to distinguish stars of the two oldest populations of the Galaxy, the thick disk and the halo. The quantity to be observed is the [Al/Mg] abundance ratio which is found to stay below −0.1 in halo stars, and above that limit in the thick disk. This cri-

terion still holds in an approximate way when abundances are determined assuming LTE, although it is then shifted to –0.45.

Due to the strong influence of NLTE effects in the atmospheres of metal-poor stars these abundances cannot be determined in a reliable way assuming LTE. There occurs a step-like change of the [Al/Mg] ratio between the two populations, which is not reproduced in the other neutron-rich light element, sodium. [Na/Mg] varies smoothly with the overall metal abundance behaving like a typical secondary element. The [Na/Mg] ratio is therefore inappropriate to detect a star's population membership.

The other typical properties of Galactic stellar populations, kinematics and age, generally confirm the [Al/Mg] classification, although with much less significance. This is not surprising if thick disk and halo are essentially coeval, as was suggested by Fuhrmann (2004). It is also compatible with the notion of kinematic properties following a broad distribution of velocities.

Whereas the observed [Na/Mg] ratios are well explained by carbon burning as described in Timmes et al. (1995), nucleosynthesis of aluminium requires a discontinuous enrichment, possibly indicating two different sites of element production.

References

Ali A.W., Griem H.R. 1965, Phys. Rev. 140,1044
Ali A.W., Griem H.R. 1966, Phys. Rev. 144, 366
Alonso A., Arribas S., Martínez-Roger C. 1996, A&AS 117, 227
Arnett, W.D., Truran J.W. 1969, ApJ 157, 339
Arnett, W.D. 1971, ApJ 166, 153
Arnett, W.D. 1996, Supernovae and Nucleosynthesis, Princeton Univ. Press, Princeton, New Jersey
Arnone E., Ryan S.G., Argast D. et al. 2005 A&A 430, 507
Asplund M., Grevesse N., Sauval A.J. 2005, ASP Conf. Series 336, 25
Baade W. 1944, ApJ 100,137
Bahcall J.N., R.M. Soneira 1984, ApJS 55, 67
Bahcall J.N.,Ratnatunga, K.U., Buser R. et al. 1985, ApJ 299, 616
Bahcall J.N., Serinelli A.M., Basu S. 2005a, ApJ 621, L85
Bahcall J.N., Basu S., Serinelli A.M. 2005b, ApJ 631, 1281
Barklem P.S., Piskunov N., O'Mara B.J. 2000, A&A 363, 1091
Baumüller D., Gehren T. 1997, A&A 325, 1088
Baumüller D., Butler K., Gehren T. 1998, A&A 338, 637
Bensby T., Feltzing S., Lundström I. et al. 2005, A&A 433, 185
Beveridge R.C., Sneden C. 1994, AJ 108, 285
Blackwell D.E., Lynas-Gray A.E. 1997, A&AS 129, 505
Böhm-Vitense E. 1958, Z. Astrophys. 46, 108
Caretta E., Gratton R.G., Sneden C. 2000, A&A 356, 238
Carney B.W., Latham D.W., Laird J.B. et al. 1994, AJ 107, 2240
Christlieb N., Gustafsson B., Korn A.J. et al. 2004, ApJ 603, 708
Cohen J., Christlieb N., McWilliam A. et al. 2004, ApJ 612, 1107
Drawin H.W. 1968, Z.Physik 211, 404
Drawin H.W. 1969, Z. Physik 225, 483

Edvardsson B., Andersson J., Gustafsson B. et al. 1993, A&A 275, 101
Eggen, O.J., Lynden-Bell, D., Sandage, A. 1962, ApJ 136, 748
Frebel A., Aoki W., Christlieb N. et al. 2005, Nature 434, 871
Fuhrmann K., 1998, A&A 338, 161
Fuhrmann K., 2004, AN 325, 3
Fuhrmann, K., Axer, M., Gehren, T. 1993, A&A 271, 451
Gehren T., Reile C., Steenbock W. 1991, in Stellar Atmospheres: Beyond Classical Models, eds. L. Crivellari, I. Hubeny and D.G. Hummer, Kluwer, Dordrecht, p. 387
Gehren T., Liang Y.C., Shi J.R., Zhang H.W., Zhao G., 2004, A&A 413, 1045 (Paper I)
Gilmore G., Reid N. 1983, MNRAS 202, 1025
Gratton R., Carretta E., Matteucci F., Sneden C. 2000, A&A 358, 671
Gratton R.G., Carretta E., Desidera S., Lucatello S., Mazzei P., Barbieri M., 2003, A&A 406, 131
Grupp F. 2004a, A&A 420, 289
Grupp F. 2004b, A&A 426, 309
Halbwachs J.L., Mayor M., Udry S. et al. 2003, A&A 397, 159
Hogg D.W., Blanton M.R., Roweis S.T. et al. 2005, ApJ 629, 268
Jonsell K., Edvardsson B., Gustafsson B. 2005, A&A 440, 321
Korn A., Shi J.R., Gehren T., 2003, A&A 407, 691
Kurucz R.L. 1992, Rev. Mex. Astron. Astrof. 23, 45
Laird J.B., Rupen M.P., Carney B.W. et al. 1988, AJ 96, 1908
Latham D.W., Stefanik R.P., Torres G. et al. 2002, AJ 124, 1144
Lindgren H., Ardeberg A. 1996, A&AS 119, 25
Mashonkina L., Gehren T., Travaglio C., Borkova T., 2004, A&A 397, 275
McWilliam A., Preston G.W., Sneden C. et al. 1995, AJ 109, 2757
Norris, J.E., 1986, ApJS 61, 667
Oort J.H. 1926, Obs. 49, 302
Perryman M.A.C. et al., 1997, A&A 323, L49
Prochaska J.X., Naumov, S.O. et al. 2000, AJ 120, 2513
Richard O., Michaud G., Richer J. et al. 2002a, ApJ 568, 979
Richard O., Michaud G., Richer J. 2002b, ApJ 580, 1100
Roman N.G. 1955, ApJS 2, 195
Ryan S.G., Norris J.E., Beers T.C. 1996, ApJ 471, 254
Salaris M., Groenewegen M.A.T., Weiss A. 2000, A&A 355, 299
Shchukina N.G., Trujillo Bueno J., Asplund M. 2005, ApJ 618, 939
Smith G., Lambert D.L., Nissen P.E. 1998, ApJ 506, 405
Spergel D.N., Verde L., Peiris H.V. et al. 2003, ApJS 148, 175
Timmes F.X., Woosley S.E., Weaver T.A. 1995, ApJS 98, 617
Truran J.W., Arnett W.D. 1971, Ap. Space Sci. 11, 430
Tsujimoto T., Shigayama T., Yoshii Y., 2002, ApJ 565, 1011
VandenBerg D.A., Swenson F.J., Rogers F.J. et al. 2000, ApJ 532, 430
Wallerstein, G. 1961, ApJS 6, 407
Woosley S.E., Weaver T.A. 1982, in Essays on Nuclear Astrophysics, eds. C.A. Barnes, D.D. Clayton & D.N. Schramm, Cambridge Univ. Press, p.377
Woosley S.E., Weaver T.A. 1995, ApJS 101, 181
Zhao G., Gehren T., 2000, A&A 362, 1077